

Tracing the strength of the South-West monsoon using boron isotopes in the Eastern Arabian Sea

Sushant S. Naik and P. Divakar Naidu
CSIR-National Institute of Oceanography, India

Gavin L. Foster and Miguel A. Martínez-Botí
Ocean and Earth Science, National Oceanography Centre Southampton, University of Southampton,
SO14 3ZH, UK

Corresponding author: S. S. Naik, CSIR-National Institute of Oceanography, Goa 403004, India
(sushant@nio.org)

Key Points

- The eastern Arabian Sea was largely an atmospheric carbon dioxide sink later to ~14 kyr.
- $\Delta p\text{CO}_2$ was briefly in excess during the deglaciation.
- Downcore salinity is significantly correlated to $\Delta p\text{CO}_2$.

Abstract

[1] Here we present the first boron isotope-based $p\text{CO}_2^{\text{sw}}$ ($p\text{CO}_2$ of seawater) reconstruction from the eastern Arabian Sea using the planktic foraminifera species *Globigerinoides ruber*. Our results from sediment core AAS9/21 show that $p\text{CO}_2^{\text{sw}}$ varied between ~160 to 300 μatm during the last 23 kyr. $\Delta p\text{CO}_2$, the sea-air $p\text{CO}_2$ difference, is relatively small during the last glacial maximum and becomes more negative toward the Holocene, with the exception of a significant excess during the last deglaciation centred on the Bølling-Ållerød. Throughout the record $\Delta p\text{CO}_2$ is predominantly negative, probably as a result of enhanced biological productivity (and higher nutrient and carbon utilization) during the south-west (SW) monsoon. A reduction in $\Delta p\text{CO}_2$ during the last glacial maximum is therefore consistent with a reduction in the strength of this monsoon system.

Keywords: Arabian Sea, *Globigerinoides ruber*, boron isotopes, monsoon, $p\text{CO}_2$

Introduction:

Antarctic ice-core records indicate that the concentration of atmospheric CO₂ during the last 800,000 years has fluctuated between 180 ppm and 280 ppm, in step with the waxing and waning of ice sheets [Petit *et al.*, 1999]. Unravelling the causes for these observed cycles of atmospheric CO₂ requires an understanding of oceanic processes, since the ocean is the only reservoir capable of exchanging the necessarily large quantities of carbon on glacial-interglacial timescales [Sigman and Boyle, 2000]. Today, fluxes of CO₂ from the oceans are roughly balanced between regions that act as a source of CO₂ (most prominently the eastern equatorial Pacific and the north-western Arabian Sea, followed by the tropical Atlantic and Indian Oceans and the north-western subarctic Pacific) and those regions that act as CO₂ sinks (mainly in the 40-60 degree belt of both hemispheres) [Takahashi *et al.*, 2009, 2014]. These patterns are intimately linked to the delivery both of remineralised organic matter to the ocean surface from the deep ocean at sites of upwelling, and the degree to which these nutrients and carbon are utilized [Moore *et al.*, 2013]. For instance, in areas where productivity is (micro)nutrient limited such as the eastern Equatorial Pacific (Fe-limited) [Moore *et al.*, 2013], nutrients are underutilised and CO₂ outgasses from the ocean to the atmosphere. The patterns of CO₂^{sw}, and more precisely, the $\Delta p\text{CO}_2$ ($\Delta p\text{CO}_2 = p\text{CO}_2^{\text{sw}} - p\text{CO}_2^{\text{atm}}$; where $p\text{CO}_2^{\text{sw}}$ is seawater $p\text{CO}_2$ and $p\text{CO}_2^{\text{atm}}$ is the atmospheric $p\text{CO}_2$) is therefore related to the nutrient budget, and significant changes in atmospheric CO₂ can come about by altering the (micro)nutrient content of surface waters [e.g. Martin, 1990]. Consequently, such processes will leave tell-tale fingerprints on the concentration of CO₂ in the surface waters.

Reconstructing the ocean carbonate system in the past requires knowledge of any two of six carbonate system parameters (pH, CO₂, [CO₃²⁻], HCO₃⁻, Total Alkalinity-TA and Dissolved Inorganic Carbon-DIC). The boron isotopic ($\delta^{11}\text{B}$) composition of planktic foraminifera is now a well-established proxy of surface water pH [e.g. Hemming and Hanson, 1992; Sanyal *et al.*, 2001; Palmer and Pearson, 2003; Foster, 2008; Henehan *et al.*, 2013] and can be used in conjunction with other constraints to reconstruct the CO₂ content of surface water in the past.

The Arabian Sea is a unique region, with semi-annual reversal of surface water circulation between southwest (SW, summer) and northeast (NE, winter) monsoons [Wyrski, 1973]. These seasonal reversals of winds over the Arabian Sea affect surface circulation, productivity, biogenic and lithogenic fluxes, CO₂ uptake and the heat budget in the region. The eastern Arabian Sea (EAS) receives a large amount of rainfall during the SW monsoon season. Most of the SW monsoon precipitation on the Western Ghats drains into the EAS through numerous rivers and streams.

Modern observations indicate that $p\text{CO}_2^{\text{sw}}$ in the Arabian Sea as a whole is in excess of that in the atmosphere, therefore acting as a significant source of carbon dioxide [Somasunder et al., 1990]. The EAS, however, displays a distinct seasonal variability with respect to surface $p\text{CO}_2^{\text{sw}}$ distribution and CO_2 flux, with a positive sea-air flux observed during the SW monsoon [Sarma, 2003]. Low $p\text{CO}_2^{\text{sw}}$ concentrations are observed along the west coast of India [Sarma et al., 2000], where Sarma et al. [2000] measured $p\text{CO}_2^{\text{sw}}$ concentrations as low as $\sim 299 \mu\text{atm}$ (SW monsoon, 1995) from the coastal waters at $\sim 15^\circ\text{N}$, which was around $60 \mu\text{atm}$ lower than the contemporaneous atmosphere ($\sim 360 \text{ ppm}$ during 1995) [Keeling et al., 2009]. Such low CO_2 concentrations in these coastal regions of the EAS are attributed to low DIC river water runoff during the SW monsoon, coupled with high surface productivity triggered by terrigenous nutrient input [Sarma et al., 1998], as also seen in the Bay of Bengal [Kumar et al., 1996]. There is a significant correlation between salinity and $\Delta p\text{CO}_2^{\text{sw}}$ [data from Sarma et al., 2000] during the SW monsoon in the eastern Arabian Sea (Fig. 1) which potentially offers a new approach to document the strength of the SW monsoon, given that we would expect a weaker SW monsoon to be associated with higher salinity, a reduced nutrient input to the coastal regions of the EAS and a reduction in the offset between atmospheric and surface water CO_2 . Here this approach is tested for the first time with a boron isotope-based pH and $p\text{CO}_2^{\text{sw}}$ reconstruction from the EAS over the last 23 kyrs.

Methods:

The sediment core AAS9/21 was collected from a water depth of 1807m (location: $14^\circ 30.539'\text{N}$, $72^\circ 39.118'\text{E}$) and is situated below the present day Oxygen Minimum Zone (OMZ) (Fig. 1, Table 1). The age model was based on five AMS ^{14}C dates [Govil and Naidu, 2010]. The sediment sample was wet sieved ($150 \mu\text{m}$ sieve), dried and sieved again in a narrow size range of $300\text{--}355 \mu\text{m}$. Samples of $1\text{--}3 \text{ mg}$ of foraminiferal carbonate (e.g. 170 tests of *G. ruber*, $300\text{--}355 \mu\text{m}$, sensu stricto) [Wang, 2000] were cleaned following standard cleaning techniques used for boron isotope analysis [see Rae et al., 2011]. Briefly, foraminifera were crushed between glass plates and clay removal was done following the method of Barker et al., [2003]. The reductive step was not carried out [see Yu et al., 2007b] but organic material was oxidized using a 1% H_2O_2 solution (buffered with $0.1 \text{ M NH}_4\text{OH}$). Samples were then treated with 0.0005 M HNO_3 to remove any adsorbed contaminants, and dissolved in $100\text{--}300 \mu\text{l}$ of Teflon-distilled $\sim 0.15 \text{ M HNO}_3$. A small aliquot of this dissolved sample ($\sim 5\%$ by volume) was taken and analyzed for trace metal composition (including B, Ca, Mg, and Al) on a Thermo Scientific Element 2 ICP-MS following the approach detailed in Ni et al. [2007]. Here, these data are used to assess adequacy of clay removal and to generate down-core temperature

estimates (using Mg/Ca). Long term precision for Mg/Ca is 3% (2 σ) and that for B/Ca is 5% (2 σ) based on repeat measurements of in-house consistency standards. The boron isotopic composition of the foraminifers was determined at the University of Southampton on a Thermo Scientific Neptune MC-ICPMS [see *Foster, 2008* and *Henehan et al., 2013*]. External reproducibility of the MC-ICPMS $\delta^{11}\text{B}$ data is determined from a relationship between the reproducibility of the Japanese Geological Survey *Porites* coral standard JCp and ^{11}B signal intensity [as described in *Henehan et al., 2013*] and is typically <0.25‰ (at 95% confidence, 2 σ) on ~1 mg of foraminiferal CaCO_3 . B/Ca was compared to the B/Ca data generated earlier from the same core [*Naik and Naidu, 2014*] and to the $\delta^{11}\text{B}$ data. B/Ca data shows differences between the two sets, probably because the B/Ca data from *Naik and Naidu, 2014*, were measured on mixed morphotypes whereas in the present study we focused on the sensu stricto morphotype only. The B/Ca and $\delta^{11}\text{B}$ do not correlate, which raise further doubts on B/Ca as a paleo-pH proxy (see supplementary data).

The Mg/Ca ratios (Fig. 2b) were converted to SSTs using the equation $\text{SST} = (1/0.09) \cdot \text{LN}(\text{Mg/Ca}/0.38)$ [*Anand et al., 2003*]. This calibration equation provided temperature estimates (reconstructed value is 28.01°C) close to the modern values at core location (28°C) [*Sarma et al., 2000*]. Oxygen ($\delta^{18}\text{O}_c$) and carbon ($\delta^{13}\text{C}$) isotope values on the same samples were obtained from the dataset of *Govil and Naidu [2010]*. $\delta^{18}\text{O}_c$ values were corrected for continental ice volume using the dataset of *Waelbroeck et al. [2002]*. The residual $\delta^{18}\text{O}$ values thus obtained were then used to compute the oxygen isotopic composition of local seawater ($\delta^{18}\text{O}_w$) (Fig. 2c) using the Mg/Ca-derived SST by applying the equation; $\delta^{18}\text{O}_w = 0.27 + ((T - 17 + 4.59 \cdot \delta^{18}\text{O}_c)/4.59)$ [*Erez and Luz, 1983*] for *Globigerinoides sacculifer*. Based on the uncertainty estimates of Mg/Ca analyses and $\delta^{18}\text{O}_c$, an overall uncertainty estimate (2 σ) for $\delta^{18}\text{O}_w$ is $\pm 0.2\%$. The $\delta^{18}\text{O}_w$ values were then converted into salinity using the equation $S = (\delta^{18}\text{O}_{sw} + 15.2)/0.45$ [*Rostek et al., 1993*]. The salinity reconstructed from core-tops using these calibrations gave values (reconstructed value is 35.7psu) close to modern measurements (35.7psu) [*Sarma et al., 2000*].

pH was calculated from boron isotope values using the species-specific calibration for *G. ruber* adapted to the 300-355 μm size fraction [*Henehan et al., 2013*] (see equations 1 & 2) with additional inputs of SST and salinity, as these parameters influence the boric acid dissociation constant pK_B^* .

$$\text{pH} = \text{pK}_B^* - \log \left(\frac{-\delta^{11}\text{B}_{\text{SW}} - (\delta^{11}\text{B}_{\text{CaCO}_3} - a)}{\delta^{11}\text{B}_{\text{SW}} - {}^{11-10}K_B(\delta^{11}\text{B}_{\text{CaCO}_3} - a) - 1000({}^{11-10}K_B - 1)} \right) \quad 1$$

$$\delta^{11}\text{B}_{\text{borate}} = (\delta^{11}\text{B}_{\text{measured}} - 8.7 \pm 1.52) / (0.6 \pm 0.09) \quad 2$$

However, the calculated pH is only weakly dependent on these environmental parameters (0.012 pH units/1°C; 0.003 pH units/psu). The pCO₂ of seawater, pCO₂^{sw}, was further calculated using pH, SST, salinity and TA (derived from salinity using the local modern day relationship between salinity and alkalinity from the GLODAP dataset) [Key *et al.*, 2004]. We have used the R version 2.15.3 for these calculations (R Core Team, 2013). The constants used in the calculation of pCO₂^{sw} were as follows: pK*_B and KHSO₄ from Dickson [1990], the relationship between total B in seawater and chlorinity by Lee *et al.* [2010], and K₁ and K₂ carbonate dissociation constants by Leucker *et al.* [2000]. pCO₂^{sw} and propagated uncertainties were calculated using a Monte Carlo approach (n=10,000) with the following uncertainties considered for the input parameters (at 95% confidence): δ¹¹B ± 0.25‰, Mg/Ca-temperature ±1°C, calculated salinity ±1 unit, TA ±50 μmol/kg.

[8] Primary productivity in the region of the EAS where core AAS9/21 is located is highest in the SW monsoon (770 mgC m⁻² d⁻¹) followed by the winter (337–643 mgC m⁻² d⁻¹) and intermonsoon (193–199 mgC m⁻² d⁻¹) seasons [Bhattathiri *et al.*, 1996]. Primary production is found to be the highest. During this period, planktic foraminifera production is also enhanced and so the flux of *G. ruber* to the sediment increases as a result of higher food availability [Curry *et al.*, 1992]. Consequently, we envisage that any proxy signals reconstructed from *G. ruber* from AAS9/21 will be biased towards the SW monsoon (June to September). Indeed, such a seasonal bias for *G. ruber* is evident from other studies further south of the present core location [Kessarkar *et al.*, 2013].

Results and Discussion:

The boron isotopic composition of *G. ruber* at AAS9/21 shows average values of 21.9 ‰ during the glacial, and 21.4 ‰ during the early Holocene. However, this decreasing trend is interrupted by lower values of 21.2 ‰ during the deglaciation (Fig. 2a). There is an increase in SST of 1.8°C and a decrease in salinity of 0.6psu from the glacial to Holocene (Fig. 2b and 2c). Reconstructed pH averages 8.32 during the glacial, 8.23 during the deglaciation and 8.24 units during the early Holocene (Fig. 2d). The Last Glacial Maximum (LGM)-early Holocene pH change is ~0.1 units and is comparable to other pH records from the Atlantic, Pacific and Indian oceans [Yu *et al.*, 2007a; Foster, 2008; Palmer *et al.*, 2010; Henehan *et al.*, 2013]. Similarly, pCO₂^{sw} shows about an 80 μatm increase shift from the LGM to the early Holocene (Fig. 2e). pCO₂^{sw} values from core AAS9/21 are low relative to reconstructed pCO₂^{sw} from equatorial Atlantic and Pacific, Caribbean Sea or the western Arabian Sea [Palmer and Pearson, 2003; Foster, 2008; Palmer *et al.*, 2010; Henehan *et al.*, 2013] and tend to be lower than contemporaneous atmospheric CO₂ [e.g. Monnin *et al.*, 2001] (Fig. 2e). Deviating from these overall trends however is a large excursion in pCO₂^{sw} to values of ~300

μatm during the late Heinrich Stadial 1- Bølling Allerød (HS1-BA). Correspondingly during this period, SST, salinity and pH remain low.

To identify the source/sink nature of the EAS with respect to CO_2 , we have calculated the difference in pCO_2 obtained from AAS9/21 (pCO_2^{sw}) and the contemporaneous ice-core CO_2 ($\text{pCO}_2^{\text{atm}}$) record over time [Monnin *et al.*, 2001, Lemieux-Dudon *et al.*, 2010, Schmitt *et al.*, 2012], termed the ΔpCO_2 : $\Delta\text{pCO}_2 = \text{pCO}_2^{\text{sw}} - \text{pCO}_2^{\text{atm}}$ (Fig.2f). The ΔpCO_2 values exhibit a trend towards more negative values through the record, except for a brief $\sim 60 \mu\text{atm}$ excursion during the HS1-BA to more positive values (Fig. 2f). The lowest ΔpCO_2 value of $-87 \pm xx \mu\text{atm}$ was recorded at 3.67 kyr, which agrees well with modern observations in the region during the SW monsoon season ($\Delta\text{pCO}_2 = -61 \mu\text{atm}$) [Sarma *et al.*, 2000; Keeling *et al.*, 2009].

The variations in the strength of the monsoon are thought to be associated with fluctuations in solar insolation [Clemens *et al.*, 1991]. The SW monsoon is known to have weakened during the LGM [Prell *et al.*, 1980; Sirocko *et al.*, 1993; Naidu and Malmgren, 1996; Kudrass *et al.*, 2001; Anand *et al.*, 2008; Govil and Naidu, 2010, 2011] with a major intensification of the SW monsoon at the onset of the BA period. On the whole, the SW monsoon was strong through the Holocene with the exception of minor interruptions [Thamban *et al.*, 2001; Anand *et al.*, 2008; Govil and Naidu, 2011; Kessarkar *et al.*, 2013]. The resolution of our record is too low to fully resolve abrupt monsoonal variations thought to have occurred at the end of YD and during the Holocene [Kessarkar *et al.*, 2013], but is high enough to resolve the gross glacial-interglacial trends. As discussed earlier, a weaker SW monsoon is today associated with a reduced runoff and hence reduced nutrient input, and a decrease in the offset between atmospheric and surface water CO_2 . In this context, the decreasing trend we observe in ΔpCO_2 through the 23 kyr record could imply an increasing SW monsoon strength. Less negative ΔpCO_2 values observed during LGM may be related to a weak SW monsoon (Fig. 2g). An exception to this trend is the more positive ΔpCO_2 during the HS1-BA period, which likely does not result from an increase in monsoonal strength as discussed further below. The negative ΔpCO_2 values observed during the Holocene agree with the strengthening of the SW monsoon seen in other records (Fig. 2g) [Thamban *et al.*, 2001; Anand *et al.*, 2008; Kessarkar *et al.*, 2013]. As observed for the modern data (See Fig. 1c), we find that ΔpCO_2 derived from the downcore data is significantly correlated with reconstructed salinity ($r^2 = 0.69$; $n = 15$; Fig. 3) with the exception of positive ΔpCO_2 values during HS1-BA. However the slope for the spatial and temporal correlations are different, probably because of local variations in evaporation and temperature [Deshpande *et al.*, 2013]. Similar correlations between ΔpCO_2 and salinity suggests that similar processes operate during the present and the 23 kyr period. The positive correlation between

$\Delta p\text{CO}_2$ and salinity supports the role of monsoon in controlling surface water $p\text{CO}_2$. Our new $\Delta p\text{CO}_2$ record therefore agrees well with the established evolution of the SW monsoon [see *Saraswat et al.*, 2013 for a review], with lower values during the glacial suggesting reduced SW monsoon strength and higher values during the Holocene suggesting increased SW monsoon strength. .

During the Bølling-Ållerød, between 14.2 and 14.4 kyr, the highest $p\text{CO}_2^{\text{sw}}$ and lowest SSTs are observed in AAS9/21 record. With the exception of these two points, SST is positively correlated to $p\text{CO}_2^{\text{sw}}$ ($r^2 = 0.8$; $n = 15$) which mainly suggests that no significant upwelling occurred in this region over the last 23 kyr, other than during the B-A interval. A $p\text{CO}_2^{\text{sw}}$ peak at a similar timing is also observed in the equatorial Pacific [*Palmer and Pearson*, 2003; *Kubota et al.*, 2014] (Fig. 4a). Furthermore, the *G. ruber* $\delta^{13}\text{C}$ record at AAS9/21 exhibits a broad deglacial excursion to low $\delta^{13}\text{C}$ ($\sim 0.4\%$ lower) centred around the B-A interval (Fig. 4b). Such $\delta^{13}\text{C}$ excursions to lower values have been observed globally in planktic and intermediate depth benthic foraminifera during the deglaciation, and are thought to be indicative of the upwelling of a nutrient-enriched water mass of Southern Ocean origin, following renewed upwelling in that region earlier in the deglacial [See *Spero and Lea*, 2002 and references therein; *Anderson et al.*, 2009]. The drop in $\delta^{13}\text{C}$ and outgassing during the deglaciation indicates a more direct connection between the core site and the sites of upwelling in the Eastern Arabian Sea. This could be due to an enhancement of upwelling as a result of an intensification of SW monsoon during the B-A, or a change in the composition of upwelled water that is retained by the time surface water is advected/mixed to our study site. This study therefore adds to the growing body of evidence that this was possibly a global feature of surface waters during the last deglaciation.

Conclusions:

Our new boron isotope-based $p\text{CO}_2^{\text{sw}}$ reconstruction reveals that the Eastern Arabian Sea was a weak sink of atmospheric CO_2 during the LGM and its strength as a sink increased after ~ 14 kyr. The present day positive correlation between $\Delta p\text{CO}_2$ and salinity, observed during the SW monsoon appears to be valid for the last 23 kyr period. Hence the decreasing $\Delta p\text{CO}_2$ trend through the last 23 kyr is interpreted as an overall increase in SW monsoon strength through the LGM and the Holocene. This interpretation agrees well with previous independent studies [*Thamban et al.*, 2001; *Anand et al.*, 2008; *Kessarkar et al.*, 2013] and therefore adds a new method capable of tracing monsoon strength in the Indian Ocean in the geological past.

Acknowledgements. This work was funded under the fast track programme of the Science and Engineering Research Board (SERB), Department of Science Technology, India awarded to SSN

(Ref. No. SR/FTP/ES-02/2011). We thank SWA Naqvi, Director, NIO for his encouragement and support and A. L. Paropkari for providing the core samples. V.V.S.S. Sarma is acknowledged for providing the seawater data. This manuscript was significantly improved by the comments of M.J. Henehan and another anonymous reviewer. The work is a part of the GEOSINKS programme PSC0106. This is National Institute of Oceanography contribution number XXXX.

References:

1. Anand, P., H. Elderfield, and M. H. Conte (2003), Calibration of Mg/Ca thermometry in planktonic foraminifera from a sediment trap time series, *Paleoceanography*, *18*(2), 1050, doi:10.1029/2002PA000846.
2. Anand, P., D. Kroon, A. D. Singh, R. S. Ganeshram, G. Ganssen, and H. Elderfield (2008), Coupled sea surface temperature–seawater $\delta^{18}\text{O}$ reconstructions in the Arabian Sea at the millennial scale for the last 35 ka, *Paleoceanography*, *23*, PA4207, doi:10.1029/2007PA001564.
3. Anderson, R.F., S. Ali, L. I. Bradtmiller, S. H. H. Nielsen, M.Q. Fleisher, B. E. Anderson, and L. H. Burckle (2009), Wind driven upwelling in the Southern Ocean and the deglacial rise in atmospheric CO_2 , *Science*, *323*, 1443-1446, doi: 10.1126/science.1167441.
4. Barker, S., M. Greaves, and H. Elderfield (2003), A study of cleaning procedures used for foraminiferal Mg/Ca paleothermometry, *Geochem. Geophys.Geosyst.*, *4* (9), 8407, doi:10.1029/2003GC000559.
5. Bhattathiri, P. M. A., A. Pant, S. Sawant, M. Gauns, S. G. P. Matondkar, and R. Mohanraju (1996), Phytoplankton production and chlorophyll distribution in the eastern and central Arabian Sea in 1994-1995, *Curr. Sci.*, *71* (11), 857-862.
6. Clemens, S., W.L. Prell, G. Murray, G. Shimmield, and G. Weedon (1991), Forcing mechanisms of the Indian Ocean monsoon, *Nature*, *353*, 720-725.
7. Curry, W. B., D. R. Ostermann, M. V. S. Gupta, and V. Ittekkot (1992), Foraminiferal production and monsoonal upwelling in Arabian sea: evidence from sediment trap, *Geol. Soc.Spl. Pub.*, *64*, 93-106.
8. Deshpande, R.D., P.M. Muraleedharan, Raj Laxmi Singh, Bhishm Kumar, M. Someshwar Rao, Medha Dave, K.U. Sivakumar, and S.K. Gupta (2013), Spatio-temporal distributions of $\delta^{18}\text{O}$, δD and salinity in the Arabian Sea: Identifying processes and controls, *Mar. Chem.*, *157*, 144-161, doi: 10.1016/j.marchem.2013.10.001.
9. Dickson, A. G. (1990), Thermodynamics of the dissociation of boric-acid in synthetic seawater from 273.15-k to 318.15-k, *Deep-Sea Res.*, *A*, *37*, 755– 766.
10. Erez, J., and B. Luz (1983), Experimental paleotemperature equation for planktonic foraminifera, *Geochem. Cosmochim. Acta*, *47*, 1025-1031.

11. Foster, G. L. (2008), Seawater pH, pCO₂ and [CO₃²⁻] variations in the Caribbean Sea over the last 130 kyr: A boron isotope and B/Ca study of planktic foraminifera, *Earth Planet. Sci. Lett.*, 271, 254–266, doi: 10.1016/j.epsl.2008.04.015.
12. Govil, P., and P. D. Naidu (2010), Evaporation-precipitation changes in the eastern Arabian Sea for the last 68 ka: Implications on monsoon variability, *Paleoceanography*, 25, PA1210, doi:10.1029/2008PA001687.
13. Govil, P., and P. D. Naidu (2011), Variations of Indian monsoon precipitation during the last 32 kyr reflected in the surface hydrography of the Western Bay of Bengal, *Quat. Sci. Rev.*, 30, 3871–3879, doi: 10.1016/j.quascirev.2011.10.004.
14. Hemming, N. G., and G. N. Hanson (1992), Boron isotopic composition and concentration in modern marine carbonates, *Geochem. Cosmochim. Acta*, 56, 537–543.
15. Henehan, M. J., et al. (2013), Calibration of the boron isotope proxy in the planktonic foraminifera *Globigerinoides ruber* for use in palaeo-CO₂ reconstruction, *Earth Planet. Sci. Lett.*, 364, 111–122, doi: 10.1016/j.epsl.2012.12.029.
16. Keeling, R.F., S.C. Piper, A.F. Bollenbacher, and J.S. Walker (2009), Atmospheric CO₂ records from sites in the SIO air sampling network, in Trends: A Compendium of Data on Global Change, Carbon Dioxide Information Analysis Center, Oak Ridge National Laboratory, U.S. Department of Energy, Oak Ridge, Tenn., U.S.A., doi: 10.3334/CDIAC/atg.035
17. Kessarkar, P. M., V. Purnachandra Rao, S. W. A. Naqvi, and S. G. Karapurkar (2013), Variation in the Indian summer monsoon intensity during the Bølling Allerød and Holocene, *Paleoceanography*, 28, 413–425, doi:10.1002/palo.20040.
18. Key, R. M., A. Kozyr, C. L. Sabine, K. Lee, R. Wanninkhof, J. L. Bullister, R. A. Feely, F. J. Millero, C. Mordy, and T.-H. Peng (2004), A global ocean carbon climatology: Results from Global Data Analysis Project (GLODAP), *Glob. Biogeochem. Cycl.*, 18(4), GB4031, doi:10.1029/2004GB002247.
19. Kubota, K., Yokoyama, Y., Ishikawa, Y., Obrochta, S., and Suzuki, A. (2014), Larger CO₂ source at the equatorial Pacific during the last deglaciation, *Scientific Reports*, 4, 5261, doi: 10.1038/srep05261.
20. Kudrass, H. R., A. Hofmann, H. Doose, K. Emeis, and H. Erlenkeuser (2001), Modulation and amplification of climatic changes in the Northern Hemisphere by the Indian summer monsoon during the past 80 k.y., *Geology*, 29(1), 63, doi: 10.1130/0091-7613(2001)029<0063:MAAOCC>2.0.CO;2.
21. Kumar, M. D., S. W. A. Naqvi, M. D. George, and D. A. Jayakumar (1996), A sink for atmospheric carbon dioxide in the northeast Indian Ocean, *J. Geophys. Res.*, 101, 18,121–18,125.
22. Lee, K., T.-W. Kim, R. H. Byrne, F. J. Millero, R. A. Feely, and Y.-M. Liu (2010), The universal ratio of boron to chlorinity for the North Pacific and North Atlantic oceans, *Geochim. Cosmochim. Acta*, 74(6), 1801–1811, doi: 10.1016/j.gca.2009.12.027.

23. Lemieux-Dudon, B., E. Blayo, J.-R. Petit, C. Waelbroeck, A. Svensson, C. Ritz, J.-M. Barnola, B. M. Narcisi, and F. Parrenin (2010), Consistent dating for Antarctic and Greenland ice cores, *Quat. Sci. Rev.*, 29(1-2), 8-20, doi:10.1016/j.quascirev.2009.11.010.
24. Lueker, T. J., A. G. Dickson, and C. D. Keeling (2000), Ocean pCO₂ calculated from dissolved inorganic carbon, alkalinity, and equations for K₁ and K₂: validation based on laboratory measurements of CO₂ in gas and seawater at equilibrium, *Mar. Chem.*, 70, (1-3), 105-119, doi:10.1016/s0304-4203(00)00022-0.
25. Martin, J. H. (2010), Glacial-interglacial CO₂ change: the Iron Hypothesis, 5(1), 1-13, doi: 10.1029/PA005i001p00001.
26. Monnin, E., A. Indermühle, A. Dällenbach, J. Flückiger, B. Stauffer, T. F. Stocker, D. Raynaud, and J.-M. Barnola (2001), Atmospheric CO₂ Concentrations over the Last Glacial Termination, *Science*, 291, 112-114.
27. Moore, C. M. et al. (2013), Processes and patterns of oceanic nutrient limitation, *Nat. Geosci.*, 6, 701-710, doi: 10.1038/ngeo1765.
28. Naidu, P.D., and B. A. Malmgren (1996), A high-resolution record of late Quaternary upwelling along the Oman Margin, Arabian Sea based on planktonic foraminifera. *Paleoceanography*, 11, 129-140.
29. Naik, S.S., and P. D. Naidu (2014), Boron/calcium ratios in *Globigerinoides ruber*: implications for controls on boron incorporation, *Mar. Micropal.*, 107, 1-7, doi: 10.1016/j.marmicro.2014.01.004.
30. Ni, Y., G. L. Foster, T. Bailey, T. Elliott, D. N. Schmidt, P. Pearson, B. Haley, and C. Coath (2007), A core top assessment of proxies for the ocean carbonate system in surface-dwelling foraminifers, *Paleoceanography*, 22, PA3212, doi:10.1029/2006PA001337.
31. Palmer, M. R. and P. N. Pearson (2003), A 23,000-Year Record of Surface Water pH and pCO₂ in the Western Equatorial Pacific Ocean, *Science*, 300, 480-482, doi: 10.1126/science.1080796.
32. Palmer, M. R., G. J. Brummer, M. J. Cooper, H. Elderfield, M. J. Greaves, G. J. Reichert, S. Schouten, and J. M. Yu (2010), Multi-proxy reconstruction of surface water pCO₂ in the northern Arabian Sea since 29 ka, *Earth Planet. Sci. Lett.*, 295, 49-57, doi: doi:10.1016/j.epsl.2010.03.023.
33. Petit, J.R., Jouzel, J., Raynaud, D. et al. (1999), Climate and atmospheric history of the past 420,000 years from the Vostok ice core, Antarctica, *Nature*, 399, 429-436.
34. Prell, W. L., W. H. Hutson, D. F. Williams, A. W. H. Be, K. Geitzenauer, and B. Molino (1980), Surface circulation of the Indian Ocean during the last glacial maximum: Approximately 18,000 ye BP, *Quat. Res.*, 14, 309-336, doi:10.1016/0033-5894(80)90014-9.
35. R Core Team (2013), R: A language and environment for statistical computing. R Foundation for Statistical Computing, Vienna, Austria. ISBN 3-900051-07-0, URL <http://www.R-project.org/>.

36. Rae, J. W. B., G. L. Foster, D. N. Schmidt, and T. Elliott (2011), Boron isotopes and B/Ca in benthic foraminifera: Proxies for the deep ocean carbonate system, *Earth Planet. Sci. Lett.*, 302(3-4), 403-413, doi:10.1016/j.epsl.2010.12.034.
37. Rostek, F., G. Ruhlandt, F. C. Bassinot, P. J. Muller, L. D. Labeyrie, Y. Lancelot, and E. Bard (1993), Reconstructing sea surface temperature and salinity using $\delta^{18}\text{O}$ and alkenone records, *Nature*, 364, 319–321, doi:10.1038/364319a0.
38. Sanyal, A., J. Bijma, H. Spero, and D. W. Lea (2001), Empirical relationship between pH and the boron isotopic composition of Globigerinoides sacculifer: Implications for the boron isotope paleo-pH proxy, *Paleoceanography*, 16(5), 515-519.
39. Saraswat, R., R. Nigam, T. Correge (2013), A glimpse of the Quaternary monsoon history from India and adjoining seas, *Palaeogeogr. Palaeoclimatol. Palaeoecol.*, 397, 1-6, doi: 10.1016/j.palaeo.2013.11.001
40. Sarma, V. V. S. S., M. D. Kumar, and M. D. George (1998), The central and eastern Arabian Sea as a perennial source of atmospheric carbon dioxide, *Tellus, Ser.B*, 50, 179–184.
41. Sarma, V. V. S. S., M. D. Kumar, M. Gauns, and M. Madhupratap (2000), Seasonal controls on surface pCO₂ in the central and eastern Arabian Sea, *Proc. Indian Acad. Sci. (Earth Planet. Sci.)*, 109(4), 471- 479.
42. Sarma, V. V. S. S. (2003), Monthly variability in surface pCO₂ and net air-sea CO₂ flux in the Arabian Sea, *J. Geophys. Res.*, 108(C8), 3255, doi:10.1029/2001JC001062.
43. Schmitt, J., R. Schneider, J. Elsig, D. Leuenberger, A. Lourantou, J. Chappellaz, P. Köhler, F. Joos, T. F. Stocker, M. Leuenberger, and H. Fischer (2012), Carbon Isotope Constraints on the Deglacial CO₂ Rise from Ice Cores, *Nature*, 336, 711-714, doi: 10.1126/science.1217161.
44. Sigman, D. M., and E. A. Boyle (2000), Glacial/interglacial variations in atmospheric Carbon Dioxide, *Nature*, 407, 859–869.
45. Sirocko, F., Sarnthein, M., Erlenkeuser, H., Lange, H., Arnold, M., and Duplessy, J.C. (1993), Century-scale events in monsoonal climate over the past 24,000 years, *Nature*, 364, 322–324.
46. Somasunder, K., A. Rajendran, M. D. Kumar, and R. Sen Gupta (1990), Carbon and nitrogen budgets of the Arabian Sea, *Mar. Chem.*, 30, 363-377.
47. Spero, H. J. and D.W. Lea (2002), The Cause of Carbon Isotope Minimum Events on Glacial Terminations, *Science*, 296, 522-525, doi: 10.1126/science.1069401.
48. Takahashi, T., et al. (2009), Climatological mean and decadal changes in surface ocean pCO₂, and net sea-air CO₂ flux over the global oceans, *Deep-Sea Res., Part II*, 56, 554-577, doi:10.1016/j.dsr2.2008.12.009.
49. Takahashi, T., S. C. Sutherland, D. W. Chipman, J. G. Goddard, T. Newberger and C. Sweeney (2014), Climatological Distributions of pH, pCO₂, Total CO₂, Alkalinity, and CaCO₃ Saturation in the Global Surface Ocean, ORNL/CDIAC-160, NDP-094, Carbon Dioxide Information Analysis Center, Oak Ridge National Laboratory, U.S. Department of Energy, Oak Ridge, Tennessee, doi: 10.3334/CDIAC/OTG.NDP094.

50. Thamban, M., V. P. Rao, R. R. Schneider, and P. M. Grootes (2001) Glacial to Holocene fluctuations in hydrography and productivity along the southwestern continental margin of India, *Palaeogeogr. Palaeoclimatol. Palaeoecol.*, 165, 113–127.
51. Waelbroeck, C., L. Labeyrie, E. Michel, J.C. Duplessy, J.F. McManus, K. Lambeck, E. Balbon, and M. Labracherie (2002), Sea-level and deep water temperature changes derived from benthic foraminifera isotopic record, *Quat. Sci. Rev.*, 21, 295–305.
52. Wang, L. (2000), Isotopic signals in two morphotypes of *Globigerinoides ruber* (white) from the South China Sea: implications for monsoon climate change during the last glacial cycle, *Palaeogeogr. Palaeoclimatol. Palaeoecol.*, 161, 381–394
53. Wyrтки, K. (1973), Physical oceanography of the Indian Ocean, in *The Biology of the Indian Ocean*, edited by B. Zeitzschel, pp. 18-36, Berlin: Springer Verlag.
54. Yu, J., H. Elderfield, and B. Hönisch (2007a), B/Ca in planktonic foraminifera as a proxy for surface seawater pH, *Paleoceanography*, 22, PA2202, doi:10.1029/2006PA001347.
55. Yu, J., H. Elderfield, M. Greaves, and J. Day (2007b), Preferential dissolution of benthic foraminiferal calcite during laboratory reductive cleaning, *Geochem. Geophys. Geosyst.*, 8, Q06016, doi:10.1029/2006GC001571.
56. Zeebe, R. E., and D. Wolf-Gladrow (2001), *CO₂ in Seawater: Equilibrium, Kinetics, Isotopes*, Oceanogr. Ser., vol. 65, Elsevier, New York.

Tables:

Table 1: Down core data for Core AAS9/21.

Age	Mg/Ca (mmol /mol)	Reconst ructed Temp (°C)	$\delta^{18}\text{O}$ (‰) Govil and Naidu, 2010	Reconst ructed Salinity (psu)	Alkali nity ($\mu\text{mol}/$ kg)	$\delta^{11}\text{B}$ borate (‰)	pK_B^+	pH	$p\text{CO}_2$ sw (μatm)	$p\text{CO}_2$ atm (μatm)	$\Delta p\text{CO}_2$ ²
3.7	4.73	28.01	-2.32	34.52	2336	21.5	8.56	8.29	186.3	272.5	-86.2
6.3	5.13	28.93	-2.21	35.15	2336	20.7	8.55	8.22	233.6	261.2	-27.6
7.4	4.89	28.39	-2.00	35.30	2339	20.8	8.55	8.23	224.0	260.4	-36.3
8.5	5.02	28.67	-1.76	35.85	2343	20.4	8.55	8.20	254.9	259.6	-4.7
8.9	4.74	28.04	-1.84	35.22	2345	20.9	8.56	8.24	219.0	261.2	-42.1
11.2	4.91	28.44	-1.75	35.13	2359	20.8	8.55	8.24	222.9	264.1	-41.2
12.2	4.42	27.27	-1.58	34.65	2366	21.0	8.56	8.27	202.3	246.5	-44.2
13.3	4.60	27.71	-1.08	35.68	2373	20.9	8.56	8.25	218.7	237.5	-18.8
14.2	4.07	26.34	-1.09	34.77	2379	19.2	8.57	8.14	297.9	238.6	59.3
14.4	4.51	27.48	-0.90	35.69	2381	19.6	8.56	8.15	292.5	239.1	53.4
15.2	5.02	28.68	-0.76	36.41	2386	20.9	8.55	8.24	227.3	225.6	1.6
17.2	3.97	26.07	-0.50	35.50	2396	21.7	8.58	8.32	172.7	192.6	-20.0
19.2	4.51	27.48	-0.29	36.52	2402	21.4	8.56	8.28	198.2	189.3	8.9
20.3	3.99	26.13	-0.85	34.61	2403	22.0	8.57	8.35	156.5	186.8	-30.4
21.3	3.80	25.58	-0.32	35.55	2403	22.0	8.58	8.35	160.6	186.0	-25.3
22.4	4.48	27.42	-0.44	36.21	2402	21.6	8.56	8.30	188.4	192.7	-4.3
23.4	4.31	26.89	-0.91	36.60	2400	21.7	8.56	8.31	183.0	190.9	-7.9

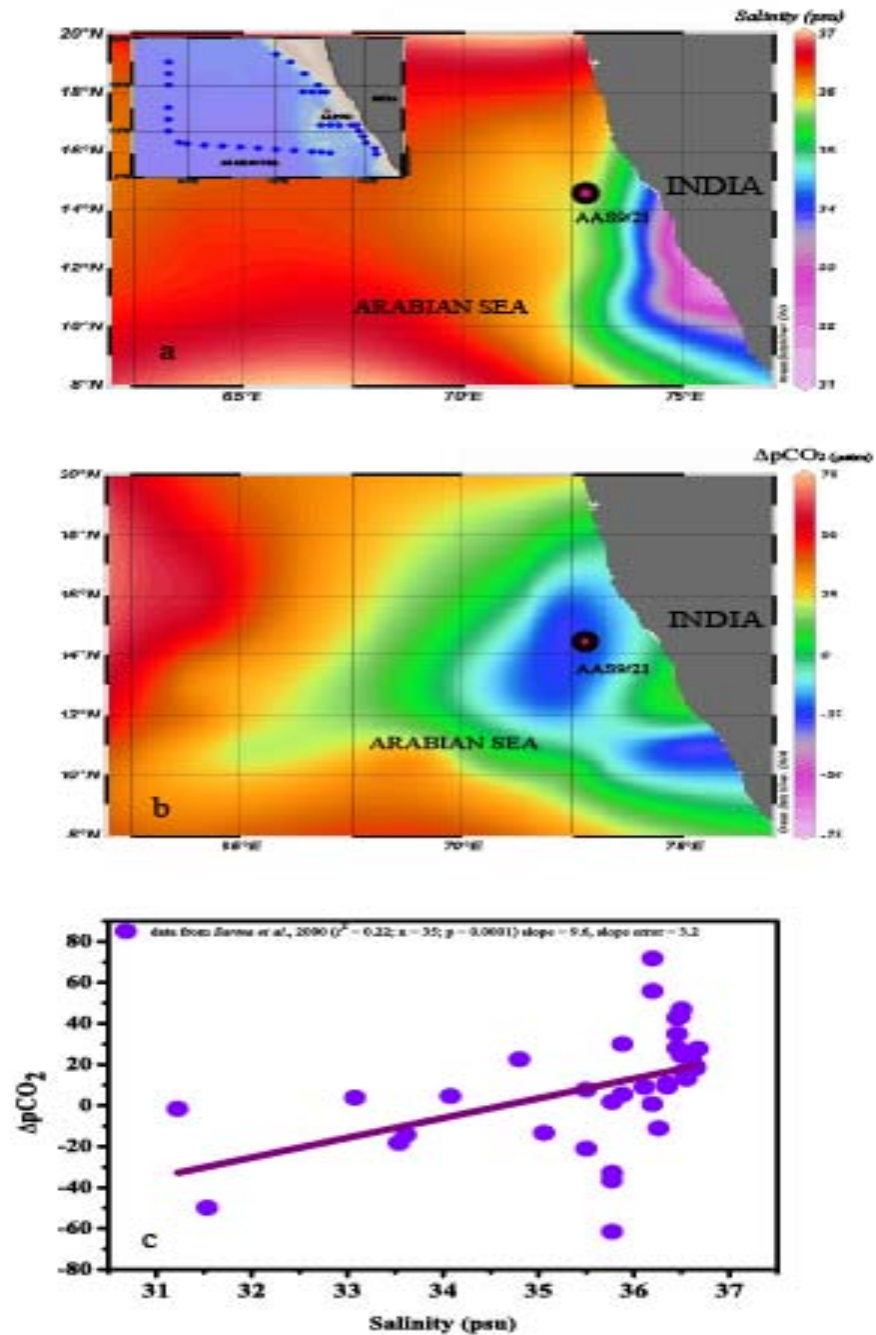


Fig. 1. a) plot of salinity and b) ΔpCO_2 , measured during July-August 1995 (south-west monsoon) [Sarma *et al.*, 2000]. ΔpCO_2 was calculated from pCO_2 and the annual average atmospheric pCO_2 during 1995 [Keeling *et al.*, 2009]. The station locations are shown in the inset picture. The AAS9/21 core is shown as a thick circle and is located in a region of negative ΔpCO_2 , i.e. atmospheric CO_2 drawdown, c) crossplot between ΔpCO_2 versus measured salinity showing a significant positive correlation.

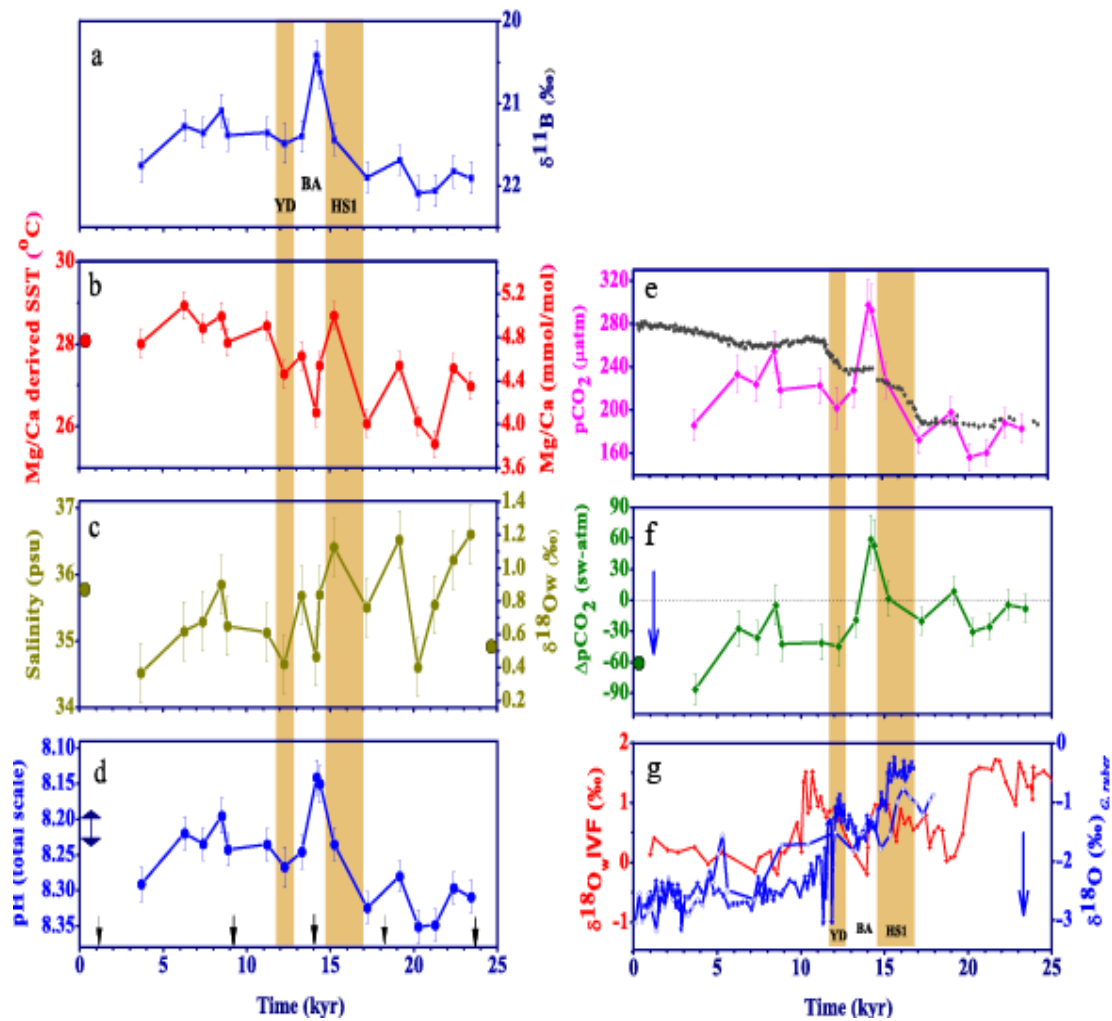


Fig. 2. Eastern Arabian Sea (EAS) sediment core AAS9/21; a) *G. ruber* $\delta^{11}\text{B}$ (‰). Error bars display 2sd error of $\sim \pm 0.2\%$, b) Mg/Ca from *Globigerinoides ruber* and Mg/Ca derived Sea Surface Temperature (SST; $^{\circ}\text{C}$) using the *G. ruber* 250-350 μm , equation from Anand *et al.* [2003]. Error bars display 2sd error of $\sim \pm 0.3^{\circ}\text{C}$ on SST c) The $\delta^{18}\text{O}_w$ derived from $\delta^{18}\text{O}_c$ of *G. ruber* after correction for ice volume [Waelbroeck *et al.*, 2002], and $\delta^{18}\text{O}_w$ calculated using the *G. sacculifer* equation by Erez and Luz [1983], Salinity (psu) was reconstructed using $\delta^{18}\text{O}_w$ using the equation by Rostek *et al.* [1993]. The uncertainty calculated on salinity is $\sim \pm 0.44$ psu, d) pH reconstructed using equations by Zeebe and Wolf-Gladrow [2001], SST and salinity (see text for details). The uncertainty calculated on pH is approximately $\sim \pm 0.02$ units, e) pCO_2 calculated using pH, SST, salinity and alkalinity (see text for details). The average uncertainty on pCO_2 is $\sim \pm 20$ μatm . A prominent pCO_2 peak is seen during late Heinrich Stadial 1- Bølling Ållerød (HS1-BA). CO_2 record from Dome C (grey dots) is plotted for comparison [Monnin *et al.*, 2001, Lemieux-Dudon *et al.*, 2010, Schmitt *et al.*, 2012], f) ΔpCO_2 , calculated as the difference between pCO_2 of seawater (as shown above) and CO_2 from Dome Concordia ice core, Antarctica. The open green circle denotes the modern ΔpCO_2 values and, g) eastern Arabian Sea proxy records depicting SW monsoon strength shown as $\delta^{18}\text{O}$ (‰) of *Globigerinoides ruber* [blue curve with stars, Thamban *et al.*, 2001; blue curve with open circles, Kessarkar *et al.*, 2013], $\delta^{18}\text{O}_w$ Ice Volume Free (‰) [Anand *et al.*, 2008]. The direction of blue arrows represents an increase in SW monsoon strength on all panels. YD = Younger Dryas, BA = Bølling Ållerød, and HS1 = Heinrich Stadial 1. Dots marked along the y-axis denote modern values of the respective parameters at the core location. The arrow marked on panel (d) shows the range of pre-industrial pH at core location. The ^{14}C dates on the core are indicated by black arrows on the bottom axis,

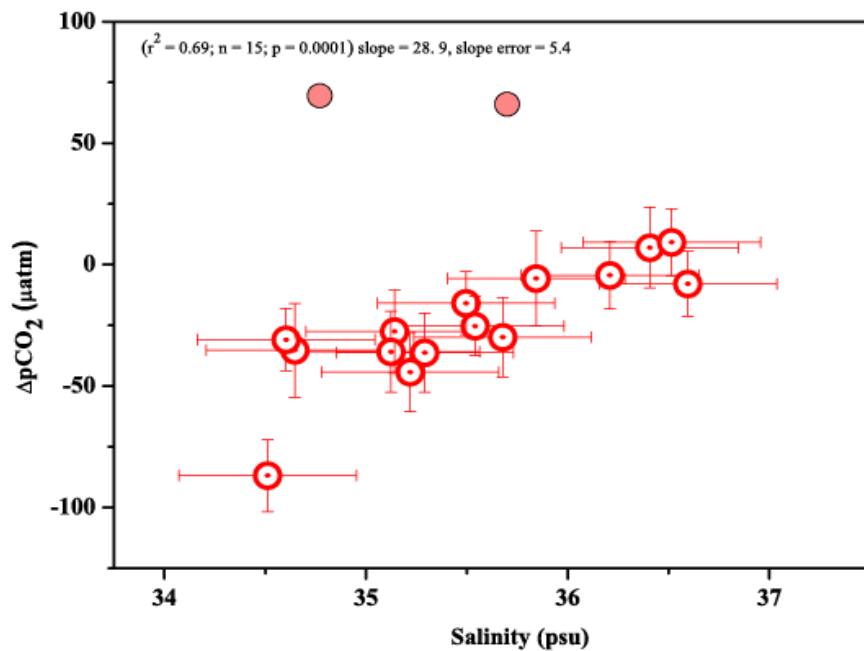


Fig. 3. Crossplot between $\Delta p\text{CO}_2$ and salinity shows significant positive correlation suggesting the role of monsoon in controlling surface water $p\text{CO}_2$. The high $\Delta p\text{CO}_2$ during HS1-BA, represented by filled circles are not included in the correlation.

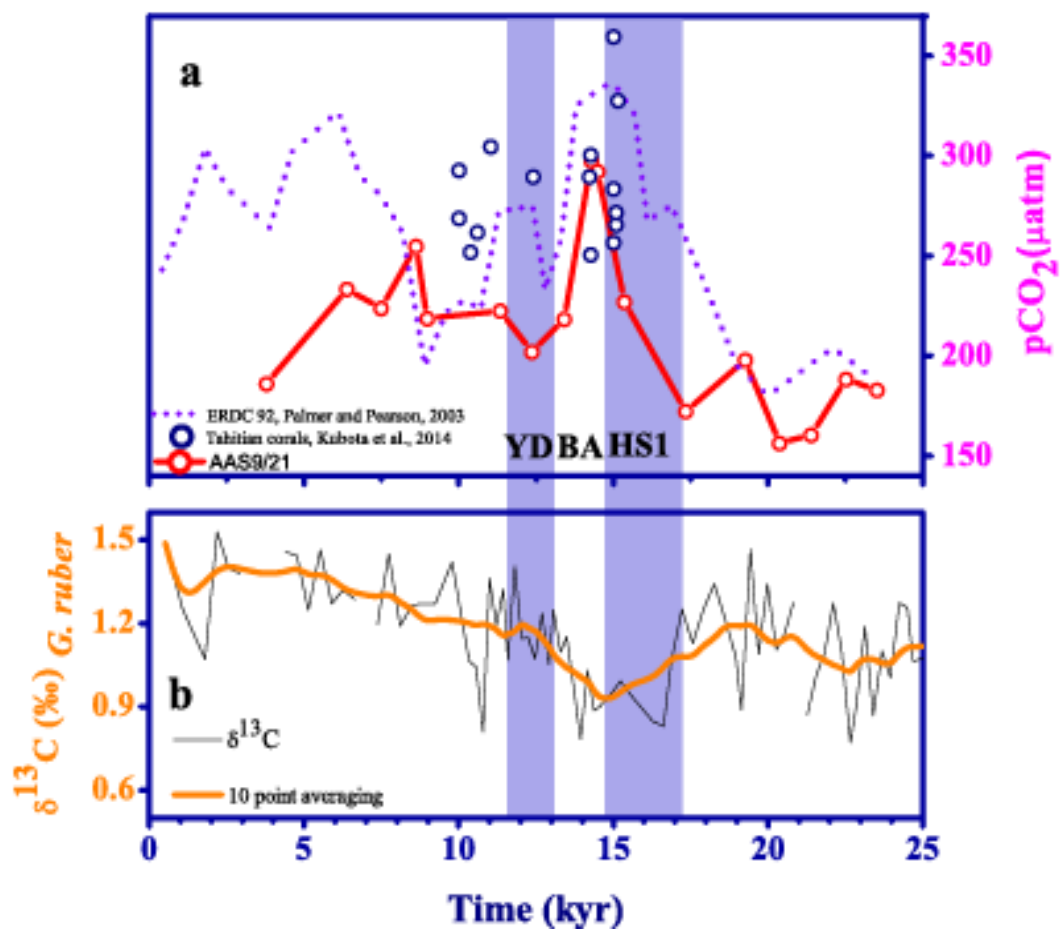


Fig. 4. pCO₂ record from AAS9/21 (thick line) compared to the pCO₂ record from the western equatorial Pacific Core ERDC-92 (dotted line) [Palmer and Pearson, 2003] and pCO₂ derived from Tahitian corals (open circles) [Kubota et al., 2014], and b) δ¹³C (‰) of *G. ruber* from Core AAS9/21.